ELSEVIER

Progress in Quantum Electronics 34 (2010) 173–190

Progress in Quantum Electronics

www.elsevier.com/locate/pquantelec

Review

Extreme ultraviolet lithography with table top lasers

M.C. Marconi[a,*], P.W. Wachulak[b]

[a]*NSF ERC for Extreme Ultraviolet Science & Technology and Department of Electrical and Computer Engineering, Colorado State University, USA*

[b]*Military University of Technology, Institute of Optoelectronics, ul. Gen. S. Kaliskiego 2, 00-908 Warsaw, Poland*

Abstract

Compact extreme ultraviolet (EUV) lasers with "table top" footprints which can be easily installed in a small laboratory environment, had enabled in the last years applications that so far had been restricted to large synchrotron facilities. The high brightness and degree of coherence of these laser sources make them a good alternative for applications where a coherent illumination is required. One of these applications is nano-photolithography realized by interferometric or "holographic" lithography. This paper describes the advances and capabilities of compact photolithographic systems based on "table top" EUV lasers.

Keywords: Nanopatterning; Interferometric lithography; EUV lasers

Contents

*Corresponding author.
E-mail address: marconi@engr.colostate.edu (M.C. Marconi).

0079-6727/$ - see front matter © 2010 Elsevier Ltd. All rights reserved.
doi:10.1016/j.pquantelec.2010.03.001

1. Introduction

Interesting and frequently technologically important phenomena occur when the dimensions of a system are sufficiently small that it becomes necessary to take into account fundamental physical, chemical, or biological processes that in macroscopic systems may be ignored. These processes include effects like the ballistic movement of an electron in a semiconductor [1], the ballistic phonon effect that reshapes the heat transfer concept in nanostructures [2,3], the unique phenomena related with near- and far-field diffraction of visible light and the excitation of collective resonances [4–7], among others. Structures with nanometer scale dimensions, where these effects become evident, are referred as nano-systems, having characteristic lengths between 1 and 100 nm. In this scale they are small enough for quantum mechanical effects to become dominant. The fundamental study of the phenomena that occur in structures having these small dimensions has given rise to a new research field that is referred to as "nanoscience".

The advancement of nanosciences had relied and will depend on our capability to fabricate structures and manipulate objects with nanometer dimensions. A clear example is the important role that nanofabrication has in the microelectronic industry. In micro-electronics the basic concept is that smaller means always better: better packaging, faster response, lower cost, lower power consumption, in summary an overall higher performance. The optimization of the electronic devices following this guiding concept has motivated the investment of an immense amount of resources from the principal players in the industry to miniaturize the components and optimize their performance. With this motivation the mass production of integrated circuits will soon start utilizing extreme ultraviolet (EUV) light for the photolithographic process, and thus had required the development of expensive and extremely sophisticated lithographic tools that probably are in the leading edge of the technological achievements of human kind. However, there are many low volume nanofabrication needs that do not fit with the large volume production scheme of these sophisticated machines. In general these nanofabrication needs are related to basic research and prototyping in academia and small scale industries. This small volume fabrication falls off the capabilities and purpose of the large machines used in mass production and needs of an alternative simpler and cost effective solution.

Examples of this low volume nanofabrication needs are periodic nanostructures in the form of gratings or arrays of pillars or holes, which are of particular interest to fabricate UV polarizers [8,9], plasmonic structures [10–13], photonic crystals and nanophotonics materials [14,15], high density magnetic memories [16,17], miniaturized RF oscillators [18], or for printing of nanometer period gratings used to evaluate the ultimate resolution of new photoresists developed for the industrial lithographic processes [19–22]. These are few examples of applications where a versatile, low volume nanofabrication capability will significantly contribute to the advancement of the field providing a fast, reliable and cost effective method to fabricate nanostructures.

Electron beam lithography and focused ion beam lithography are excellent ways to realize nanostructures with periods below 100 nm. These tools are probably the most versatile solution of nanoscale prototyping [23]. However, due to their intrinsic serial characteristic the nanostructure must be fabricated with a pen-like tool, and consequently they are time consuming and not very well suited for large area patterning. Other low volume fabrication alternatives include self-assembly, replication by embossing, molding or printing with master stamps. These approaches increase the area over which the

nanostructures are fabricated [24–27]. However, they have some limitations. In the case of self-assembly, the arrangement of nanostructures is frequently organized in reduced areas or domains which are very difficult to control, while in the replication by master stamps, different motifs require different master stamps, restricting the versatility of the method.

Interferometric lithography (IL), also referred as holographic lithography is an attractive alternative for efficient, versatile low-volume patterning of periodic structures over large areas. In IL, the lithographic step is achieved combining mutually coherent light beams at the surface of a photoresist coated substrate. The interference pattern created in this way produces a sinusoidal profile with a period

$$d = \frac{\lambda}{2\sin\theta} \tag{1}$$

where λ is the wavelength and θ the half angle between the intersecting beams. The intensity distribution produced by interference activates the photoresist deposited in the sample and generates the nanostructure that defines the lithographic mask necessary in the next steps of the fabrication process.

One dimensional periodic patterns or gratings are the simplest structures that can be fabricated with this method. Some flexibility can be obtained with a little more sophisticated set ups, for example combining more than two beams to generate the interference pattern or making multiple exposures, changing the exposure conditions and/or orientation of the sample in each exposure. These more elaborated set ups allow for the generation of two dimensional arrays of nanostructures. For example, a multiple exposure approach combined with the control of the phase of the interfering beams allows for more complex 2D structures [28]. Also multiple beams IL, obtained by especially designed diffraction gratings masks, generates 2D arrays of holes or pillars arranged in rectangular or circular patterns [29–32]. Sub-wavelength (22 nm half pitch) triangular groves were fabricated in Si using a self-aligned technique defined as spatial frequency doubling [33].

In principle, it is valid to say that the size of the smallest feature that can be obtained using a photon-based lithographic tool is determined by the wavelength λ used in the photolithographic step and the numerical aperture (NA) of the optics used for the printing

$$\delta = \frac{k\lambda}{NA} \tag{2}$$

where k is a constant of the order of 1 that depends on the illumination characteristics [34]. This expression makes clear that one possible approach to reduce the period of the nanostructure is to increase the NA of the exposure tool. Alternatively, the other approach is to reduce the wavelength of the illumination source.

In the first approach, schemes using immersion optics had provided a direct path to increase the NA of the exposure with the purpose to decrease the period of the printed nanostructures. Hoffnagle et al. used liquid immersion IL at 257 nm wavelength to print 89 nm periodic patterns to characterize the performance of new photoresists [21,22]. Switkes and Rothschild few years later printed 60 nm period gratings using 157 nm light, proposing this technique as the way to improve the resolution of optical lithography [35,36]. The simplicity of the immersion IL approach had motivated an enormous amount of work since then, utilizing different immersion liquids and light sources [22,35,37–45].

Reduction in the smallest period that can be printed is also achieved utilizing shorter wavelength radiation, in the EUV and X-ray region. In the short wavelength region,

synchrotrons sources provide a large photon flux and tunable output. However, the spatial and temporal coherence of the beam are much lower than those typically obtained with laser sources. For IL applications it is necessary to perform additional filtering to obtain the necessary degree of spatial and temporal coherence to assure a good contrast in the interference fringes over large areas. This additional filtering has the immediate consequence of a serious flux reduction that increases the exposure time necessary to activate the photoresist. Regardless this inconvenience, synchrotrons are always an attractive short wavelength source for leading-edge IL experiments.

Other alternative for short wavelength coherent sources are compact extreme ultraviolet (EUV) lasers developed in the last decade. These newly developed laser sources open new possibilities to realize efficient nanopatterning in compact (table top size) setups with similar capabilities to systems now only accessible with synchrotron sources [46–48]. The development of EUV and soft X-ray lasers that can easily fit on an optical table facilitated the demonstration of a large number of applications including photolithography, interferometry, microscopy, holography, nano-machining, high resolution mass spectroscopy and nano-ablation [49–61].

This paper will describe in some detail a small aspect of the vast field of nanolithography. The focus of this work is to describe the realization of table top lithographic systems based on the coherent illumination from compact extreme ultraviolet lasers. Exploiting the unique characteristics of these compact EUV sources, short wavelength, high flux and excellent spatial and temporal coherence, allows for the realization of nanopatterning tools with the capability to print sub-100 nm features. The nanopatterning was demonstrated utilizing different approaches: the well established interferometric lithography technique and holographic projection lithography. Section 2 presents a detailed description of the compact extreme ultraviolet laser sources. Section 3 is devoted to the description of a wavefront division interferometric lithography tool based on a Lloyd's mirror interferometer. In Section 4, the results obtained with an amplitude division interferometer implemented with a transmission diffraction grating used as beam splitter will be discussed. Section 5 describes the results using holographic projection lithography from a computer generated binary hologram. Section 6 shows examples of nanostructures fabricated in thin metal layers where the photolithography step was performed by IL using EUV lasers. Finally, the conclusions and potential path for the future developments will be discussed.

2. Compact table top EUV lasers

Fig. 1 shows two compact EUV laser units built at Colorado State University based on a fast discharge excitation. These systems are the most compact EUV lasers available at this time. The first unit (Fig. 1a) is a "table top" laser whose head has a footprint approximately $0.7 \times 1.2\ m^2$. It is connected through a high voltage coaxial cable to a Marx generator that supplies the voltage for the discharge. The second unit (Fig. 1b) is a more compact version or "desk top" laser with even a smaller footprint ($0.8 \times 0.4\ m^2$). In this case the power supply is also more compact and can be placed below the optical table. Both lasers are based on a capillary discharge-pumped excitation scheme that produces an intense amplification at $\lambda = 46.9$ nm by excitation of "Ne-like Ar" (Ar^{+8}) ion. These are cavity-less single pass (or amplified spontaneous emission) lasers that in one pass produce a

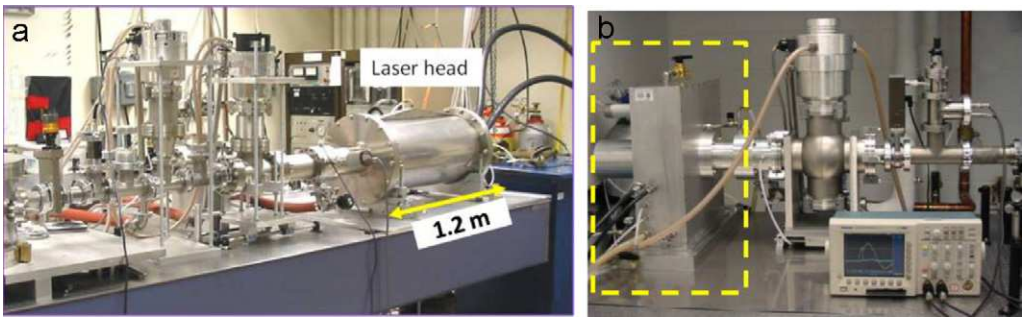

Fig. 1. Pictures of the capillary discharge EUV lasers.(a) Table top system with a footprint $1.2 \times 0.7\,m^2$. (b) "Desk top" version. The laser head is indicated by the dotted square in the picture.

collimated laser beam with the sufficient coherence and peak power to realize a robust table top nanopatterning tool.

Lasing is obtained in the 46.9 nm 3s $^1P_1$–3p $^1S_0$ ($J=0$–1) transition of the Ar^{+8} ion. An alumina capillary 3.2 mm inner diameter filled with Ar is excited with a fast current pulse having an amplitude of the order of 24 kA, a 10% to 90% rise time of $\approx$25 ns and a first half-cycle duration of $\approx$110 ns for 27 cm capillary length. The discharge parameters slightly change with the capillary length due to the variation in the discharge inductance. The fast current pulse is produced by discharging a capacitor through a low inductance circuit connected to a spark gap switch in series with the capillary load. The current pulse rapidly compresses the plasma column to form a dense and hot filamentary plasma channel where population inversion is created between the 3p($^1S_0$) and 3s($^1P_1$) levels by strong monopole electron impact excitation of the laser upper level and rapid radiative relaxation of the laser lower level. A continuous flow of Ar is injected in the front of the capillary while an optimum Ar gas pressure of 490 mTorr is maintained in the capillary channel [46,47,62].

The table top laser developed at Colorado State University produces pulses approximately 400 μJ at repetition rates up to 4 Hz [63]. The spatial coherence varies with the length of the gain medium [64,65]. For a 36 cm long gain medium, a coherence radius of 550 μm measured at 1.5 m from the source that includes almost half of the entire laser power is obtained. The coherence radius was measured analyzing the fringe visibility of the interference fringes obtained when a mask with two pinholes at different separations was placed at selected distances from the source [65,66]. The coherence radius R_c characterizes the transverse coherence of the laser beam, and was defined following the convention of coherence area used by Goodman [67]. The laser has a narrow spectral bandwidth mostly dominated by Doppler broadening, $\Delta\lambda/\lambda \leq 10^{-4}$, corresponding to a temporal coherence length of 470 μm.

Capillary discharge excitation demonstrated to be an efficient way to produce intense EUV laser radiation. After the first demonstration in Colorado State University, several groups have demonstrated EUV laser emission with systems based on a capillary discharge scheme in laboratories in Italy, China, Japan, Malaysia and the Russian Federation [48,68–72].

3. Wavefront division interferometric lithography

In this interferometer scheme the interfering beams are obtained by dividing the incoming wavefront in two or more mutually coherent beams. One example of this

approach is the multiple beams interference scheme obtained with specially fabricated diffraction masks composed of several diffraction gratings arranged in different configurations. These masks are composed of multiple gratings arranged in such a manner that the diffraction orders of the different individual gratings are recombined in the surface of the sample to produce multiple beams interference. The masks can be designed with different patterns to allow a great versatility in the shape, period and configuration of the arrays of structures that can be printed. Changing the orientation, period and number of the gratings in the mask it is possible to print arrays of holes in square, hexagonal or circular patterns [32,73–75]. Recently, using the second order diffracted orders in a two gratings mask Isoyan et al. demonstrated an improvement of 4X reduction in the printed period [76].

Another option, very attractive for its extreme simplicity, is the wavefront division Lloyd's mirror interferometer. In this interferometer, part of the laser beam impinges on a flat mirror at an incidence angle θ and is reflected to interfere with the remaining undeflected portion of the beam, as illustrated in Fig. 2. This simple scheme is a convenient configuration for IL in particular at EUV wavelengths, where the availability of high efficiency optics is a main concern. Lloyd's mirror interferometer was used with synchrotron illumination to fabricate gratings in different photoresists with sub 20 nm line widths utilizing 13.4 nm wavelength illumination [77–79].

Table top EUV lasers in combination with a Lloyd's interferometer were also used to print lines and two dimensional arrays of holes and pillars in different photoresists [51,80–82]. Both beams converge at the edge of the mirror on the sample to give rise to a sinusoidal intensity pattern of period d, defined by the wavelength of the light λ and the incidence angle θ according to Eq. (1). Fig. 3 shows a photograph of the device used in the experiment with the $\lambda = 46.9$ nm EUV laser in Colorado State University. A Cr coated flat mirror was mounted at grazing incidence in front of the laser beam on a pivoting platform, with its rotation axis coincident with the farther edge of the mirror. The pivoting platform allows to change the incidence angle θ and in this way to control the periodicity of the interference pattern. The samples were mounted at this edge of the mirror in a motorized rotation stage that allows rotation of the sample by an angle α around an axis normal to the sample's surface and parallel to the mirror's surface. This feature is used to produce two dimensional arrays of dots or holes by rotating the sample in multiple exposures experiments. The Lloyd's mirror interferometer system is extremely compact. It was housed in a small vacuum chamber ($0.45 \times 0.55 \times 0.40$ m^3) that was differentially pumped

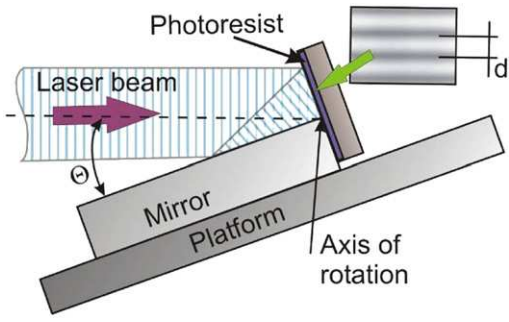

Fig. 2. Lloyd's mirror wavefront division set up. The laser beam impinges the flat mirror at an incidence angle θ.

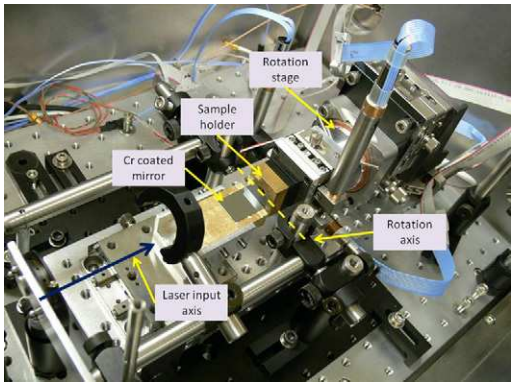

Fig. 3. Lloyd's mirror nanopatterning tool. The sample is placed at the edge of a Cr coated mirror. The whole setup can be tilted around the rotation axis. Also the sample can be rotated around an axis parallel to the mirror's surface to print 2D structures.

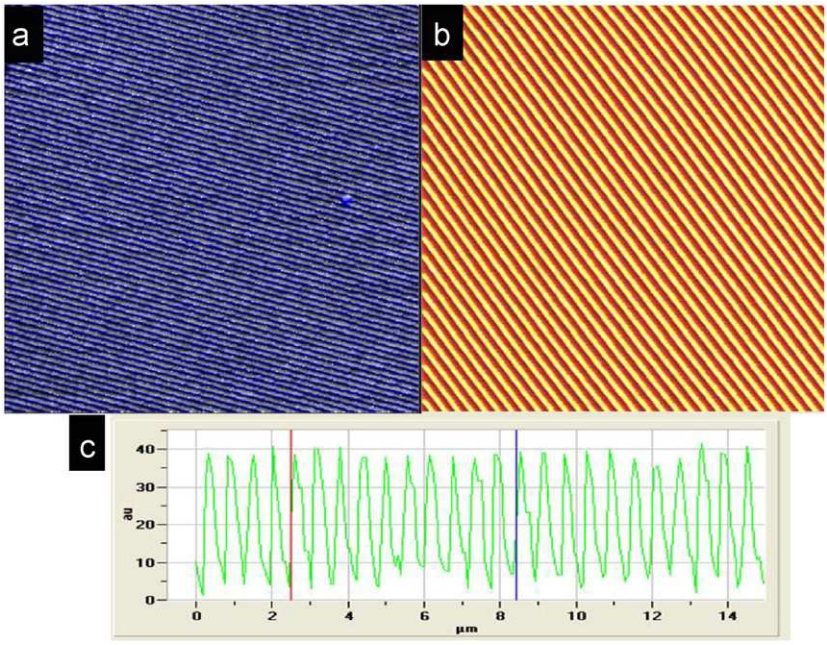

Fig. 4. Atomic force microscope micrographs of gratings printed in PMMA using the Lloyd's mirror setup. (a) 95 nm period gratings, (b) 590 nm period grating and (c) cross section of the grating shown in (b).

respect to the laser to maintain a pressure of approximately 10^{-5} Torr. All the critical movements to align and rotate the samples are controlled by vacuum compatible actuators. This allows to make multiple exposure experiments without breaking vacuum, assuring identical exposure conditions. The entire EUV IL printing tool including the laser source has a footprint of $0.7 \times 2.6\ m^2$.

With the Lloyd's mirror interferometer set up it is possible to print large area or regular lines with periods below 100 nm in a single exposure [51,77,83,84]. Fig. 4 shows atomic

force microscope micrographs of lines printed on polymethyl methacrylate (PMMA). Fig. 4a depicts lines with a period of 95 nm, Fig. 4b corresponds to lines with a larger period, approximately 590 nm. Fig. 4c is a lineout of the cross section cut across the lines with period of 590 nm. The maximum modulation observed in this structure is 22 nm, limited primarily by the absorption length of the 46.9 nm photons in the PMMA photoresist.

More versatility with this nanopatterning tool can be obtained combining several exposures in the same sample. Using a Lloyd's mirror scheme combined with multiple exposures it is possible to print different two dimensional motifs. Fig. 5 shows some examples of the nanostructures that can be printed in the photoresist using this interferometer with multiple exposures. Fig. 5a–c shows several atomic force microscope micrographs of different patterns obtained in PMMA with different rotation angles α and different incidence angle θ between the two exposures. With the sample rotation angle $\alpha = \pi/2$, symmetric dots in a square pattern are obtained as shown in Fig. 5a. If the incidence angle in the two exposures is changed, rectangular shaped dots with different periods in the x and y directions (in the surface of the sample) are obtained as shown in Fig. 5b. Maintaining the same incidence angle but changing the rotation angle of the sample to $\alpha = \pi/6$, regular elongated dots are produced instead, as those shown in Fig. 5c.

Changing the exposure dose allows another degree of freedom to switch from the fabrication of pillars to holes. With a small dose the PMMA is activated only in thin lines corresponding to the interference maxima. The superposition of two exposures develops small holes in the loci where the maxima of interference superpose. On the other hand, if the dose is increased, the PMMA is activated in wide trenches developing in the intersection of the interference minima small regions with unexposed photoresist that resembles cone-shaped nanodots.

The cone-shaped nanodots shown in Fig. 5 have a typical FWHM of 60 nm and a period of 150 nm. The height of the features printed in PMMA however is only 25–30 nm. This is a limitation imposed by the shallow penetration depth of the $\lambda = 46.9$ nm photons in the photoresist. For practical applications like fabrication of nanostructures it is necessary to transfer these patterns from the photoresist to the underlying substrate. The patterned

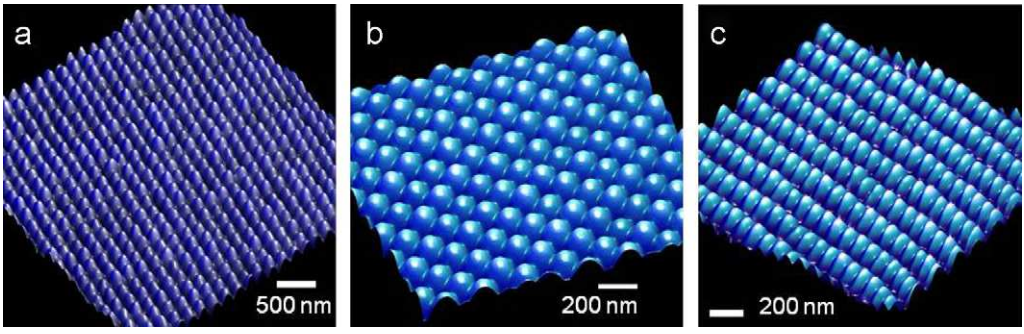

Fig. 5. Two dimensional structures printed with the Lloyd's mirror interferometer with a double exposure in PMMA. (a) Dots with a FWHM of approximately 60 nm, and a period of 150 nm. (b) Rectangular shaped dots obtained by changing the incidence angle θ between the two exposures. (c) Elongated dots obtained by rotating the sample an angle $\pi/6$ around the axis parallel to the mirror's surface.

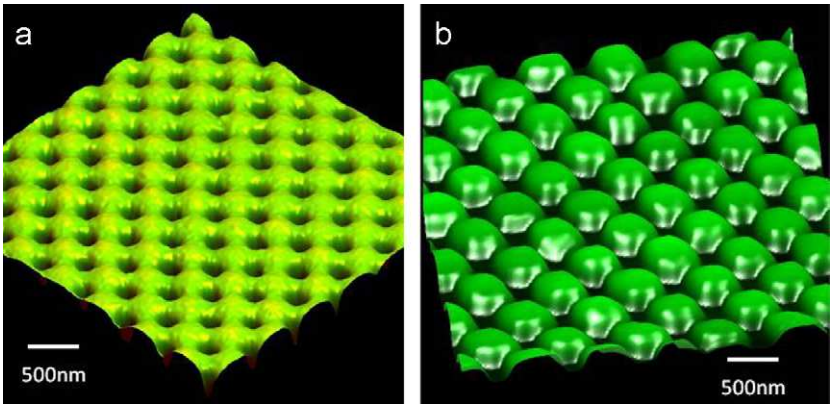

Fig. 6. (a) Array of holes 130 nm FWHM and 100 nm in depth and (b) dots printed in HSQ using the Lloyd's mirror setup.

photoresist layer is used as a lithographic mask to define the nanostructure in the substrate by further processing such as electroplating, lift-off or anisotropic etching. Thus, the extremely small thickness of the photoresist layer imposes a potential limitation for an effective nanostructure fabrication.

An alternative to get through this problem and increase the height of the structures printed in the photoresist layer is to use a different product to define the mask, such as the Si-based photoresist hydrogen silsesquioxane (HSQ). The 46.9 nm photons from the EUV laser have much larger penetration depth in this Si-based photoresist, in excess of 120 nm, allowing printing of structures with larger aspect ratio that facilitates further sample processing. Fig. 6 is an example of the thick masks that can be fabricated in HSQ. Fig. 6a shows an atomic force micrograph of an array of holes obtained with a high exposure dose. The HSQ is activated in wide strips along the maxima of interference that develops symmetric holes in the loci where the minima of interference superpose about 130 nm FWHM and 120 nm depth as shown in Fig. 6a. If the dose is reduced, a regular array of dots is obtained instead. For lower doses the photoresist is activated only in small volumes corresponding to the maxima of intensity creating the array of symmetric dots as the one shown in Fig. 6b [82].

The Lloyd's mirror configuration combined with the table top EUV laser constitutes a simple and versatile interferometric tool capable to produce photoresist masks with various features with minimal changes in the exposure conditions. All the patterns shown in Figs. 5 and 6 were obtained with typical exposure times of 1–2 min [81,82,85].

In the experiments described so far, the printed area is limited to approximately $500 \times 500\ \mu m^2$ by the spatial coherence of the laser source. This is a consequence of the wavefront division scheme of the Lloyd's interferometer that divides and folds the wavefront in the two beams to produce the interference, and consequently it requires a highly spatially coherent illumination. To find the maximum area where it is possible to achieve an interference pattern, it is necessary to analyze the coherence characteristics in the two beams. Two coherence parameters in the illumination beam must be considered is this analysis, the temporal or "longitudinal" coherence and the spatial or "transversal" coherence.

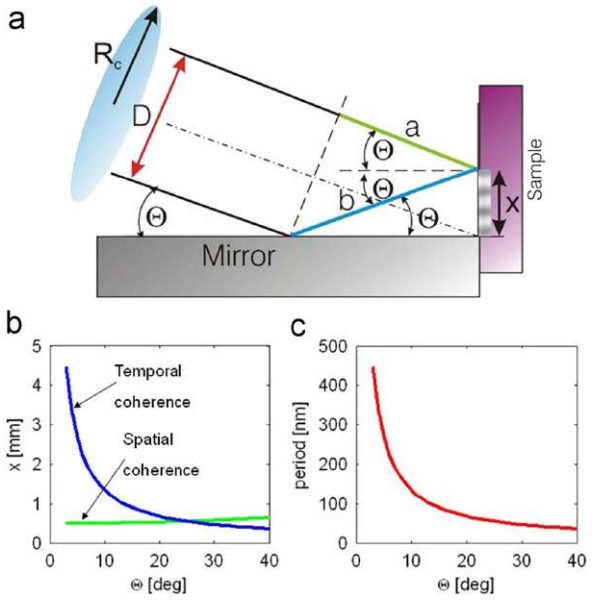

Fig. 7. (a) Scheme of the Lloyd's mirror interferometer indicating the optical path difference between the two beams ($OPD=(b-a)$). R_c represents the coherence radius which should be larger than the beam cross section in order to obtain a good interference pattern. (b) Maximum printable distance x limited by the spatial and temporal coherence as a function of the incidence angle θ indicated by the eqs (3) and (4). (c) Period of the gratings printed with the Lloyd's mirror setup as a function of the incidence angle θ.

The temporal coherence limits the printable region in the sample to a distance x (measured from the edge of the mirror) equal to

$$x \leq \frac{l_c}{2\sin\theta} \tag{3}$$

where l_c is the longitudinal coherence length, and θ the incidence angle. This limit can be calculated requiring that the optical path difference between the beam reflected from the mirror and the beam that directly illuminates the sample is smaller than the longitudinal coherence length. Fig. 7a shows these parameters and the condition indicated in formula 3 corresponds to $(b-a)\leq l_c$.

The other parameter that limits the printable area in the sample is the spatial coherence. This limits the x distance to

$$x \leq \frac{R_c}{\cos\theta} \tag{4}$$

where R_c is the radius of coherence of the input beam. This limit requires that the illuminating beam must be spatially coherent. This is indicated in Fig. 7a as the condition $D\leq 2R_c$. Fig. 7b shows the maximum printable distance limited by the spatial and temporal coherence as a function of the incidence angle θ indicated by the relations (3) and (4). It is worth to mention, however, that for 1-D pattern fabrication the second dimension of the pattern, parallel to the mirror's edge, can be in principle as large as the beam itself, typically few millimeters. Only for 2-D patterns, where the sample rotation is required, the coherence limit is imposed in both directions thus reducing the pattern area more severely.

Fig. 7c is a plot of the period of the lines that can be printed with the Lloyd's configuration, also as a function of the incidence angle θ. For the majority of applications, the region of interest corresponds to periods between ~50 and 100 nm, which can be printed with incidence angles 13–26°. The plot in Fig. 7b indicates that in this incidence angle range, the limiting factor is the spatial coherence. Above the incidence angle of 26° the temporal coherence starts to play a role in limiting the patterning width. The problem imposed by the spatial coherence can be attenuated placing the interferometer further away from the source to increase the coherence radius. However, this will immediately increase the necessary exposure time to activate the photoresist, and degrade the quality of the structures due to the increased influence of vibrations would have in an extended exposure. Another potential inconvenience of the Lloyd's mirror scheme is that the portion of the beam reflected in the mirror has a different intensity than the direct beam due to the reflectivity of the mirror. The intensity of the reflected beam decreases with increasing incidence angle, which corresponds to the smaller periods. Thus, it will be expected that the visibility of the interference fringes (or what is equivalent the modulation of the printed pattern in the photoresist) will decrease as well. An alternative approach to overcome the limitation imposed by the spatial coherence of the beam is utilizing an amplitude division interferometer that will be described in detail in the next section.

4. Amplitude division interferometric lithography

In an amplitude division interferometer (ADI) the beam spatial coherence requirement is more relaxed than in the case of wavefront division interference scheme. This is because the interference is obtained by the superposition of two beams that are replicas of the original wavefront, so every section of the interference pattern is produced by the superposition of the same section of the original beam and is consequently spatially coherent. The amplitude division interferometer schemes were used in the last years with low coherence sources to demonstrate what was denominated "achromatic" interferometric lithography. In achromatic IL the temporal coherence is not a relevant limitation and the spatial coherence only plays the role of limiting the depth of focus of the system [87–90].

We developed an ADI–IL system compatible with the EUV table top laser sources [85]. The amplitude division interferometer is constructed with a transmission diffraction grating that is used to split the incoming beam in several beams. After reflection in two folding mirrors the two first order diffraction beams are recombined in the surface of the sample, while the zero order is blocked by a central stop. Changing the incidence angle in the folding mirrors it is possible to adjust the period of the lines printed on the surface of the sample. This can be done with a linear actuator that rotates simultaneously both mirrors keeping the alignment of the interferometer unchanged.

The grating used as the beam splitter was fabricated by electron beam lithography in a 350 nm thick photoresist layer supported on a 100 nm thick Si membrane. The thick photoresist layer provides a substantial absorption to the EUV photons while the thin Si membrane has a transparency approximately 20% to the $\lambda = 46.9$ nm photons. The grating period was 2 μm with a 50% duty cycle. A scheme and a photograph of the ADI device are shown in Fig. 8.

When illuminated with a collimated beam, the grating produces two replicas of the wavefront that are mutually coherent. The alignment of this interferometer requires to superpose the two beams in the sample with accuracy better than the transverse coherence

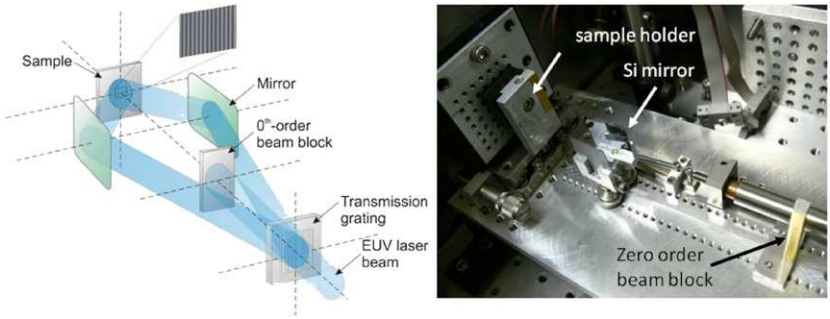

Fig. 8. Scheme and photograph of the amplitude division interferometer implemented with a transmission diffraction grating used as beam splitter and two folding mirrors to recombine the beams in the sample plane.

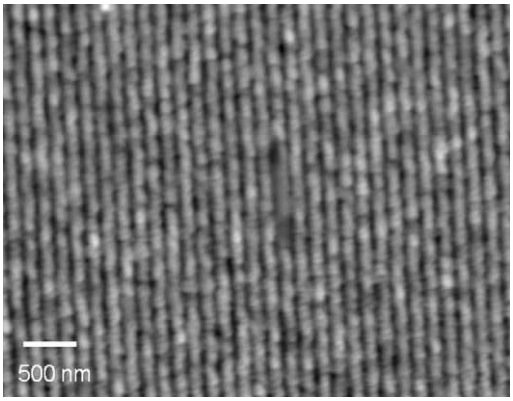

Fig. 9. 145 nm period grating printed in HSQ using the amplitude division interferometer.

length of the laser, which for our experimental conditions is a fraction of a millimeter. The optical path difference between the two interferometer branches has to be adjusted better than the longitudinal coherence, approximately 0.5 mm. In this scheme the intensities of the two first diffraction orders that produce the interference are equal, so a good fringe visibility in the interference pattern and consequently a good modulation in the printed grating should be expected.

Fig. 9 shows lines pattern with a period of 145 nm (72.5 nm thick lines) printed on HSQ with the ADI set up. The printed area is $2 \times 0.6\,\mathrm{mm}^2$, corresponding to the size of the diffraction grating used as the beam splitter in this experiment. Printed lines with smaller period, down to 95 nm, were also obtained increasing the angle between the two beams impinging at the sample. However, the 95 nm period lines showed an increased noise and lower modulation as compared to the larger periods. The lower quality of the printing can be explained if we consider several factors that contribute to the deterioration of the pattern quality by adding a background noise. One of these factors is that for this experiment we used the smaller version (“desk top”) laser that provides a substantially lower energy per pulse (about 10 μJ per pulse) [62]. This lower photon flux increased the necessary exposure time to approximately 10 min. The larger exposure time might be an explanation for the lower quality printing because vibrations during the exposure

significantly contribute to the image deterioration. In addition the print quality may possibly be affected by photoresist scumming that is particularly severe in 50% duty cycle lines with line widths approaching 50 nm, particularly for the HSQ photoresist [92]. The optical quality of the beam splitter and the folding mirrors is also a possible reason for the increased noise in the lines printed with this interferometer. The presence of scattering centers in the grating beam splitter and in the folding mirrors might introduce a random noise background reducing the fringe visibility and the quality of the patterns. Furthermore, small variations in the thickness of the Si membrane that supports the grating beam splitter can introduce random phase and intensity variations across the beam which also reduces the fringe visibility. This becomes an important contribution to the background noise if we consider the high absorption coefficient that all materials exhibit at 46.9 nm. For example, in the case of Si which is the material of the supporting membrane in the diffraction grating, a roughness of ± 10 nm around 100 nm thickness will produce a random change in the transmission (an consequently in the cross section intensity of the beam) of about 14%, introducing a severe aberration and loss of visibility [93].

5. Holographic projection

The EUV interferometric lithography systems described in the former sections are very useful for generating periodic patterns. However they are based on interference and consequently limited by its very nature to periodic structures. An extension of interferometric lithography towards arbitrary patterning is holographic lithography. In this approach a hologram is reconstructed by coherent illumination on the surface of the sample and in this way arbitrary motifs can be printed in the surface of the photoresist. This approach has been proposed some years ago by Jacobsen et al. and recently demonstrated using a 13.4 nm wavelength undulator EUV source [94–97]. However, to attain the same spatial resolution, holographic lithography requires an illumination with a larger degree of spatial and temporal coherence as compared to EUV-IL. This requirement imposes strong filtering in synchrotron sources which limits the available photon flux increasing the necessary exposure to activate the photoresist.

The holographic projection lithography approach has the advantage of a very simple set up: it consists of only a single diffractive element, a holographic binary mask that can be designed as a computer generated hologram (CGH) and a coherent illumination source. The simplicity of the experimental set up is particularly important in the EUV range where complex optical systems to form the image are particularly difficult to implement. The CGH is designed by calculating the interference pattern produced between the diffracted wave of the selected hologram motif and the reference beam. This calculation is performed applying the two-dimensional Fresnel–Kirchhoff integral, calculated using fast Fourier transformations (FFTs). Since the fabrication of the hologram is binary, a conversion from a continuous tone image produced by the calculated image to a binary image is needed, which in turn adds background noise and spurious artifacts to the final reconstructed target image. However, to reduce this harmful effect and improve the object printability, several algorithms for continuous tone conversion, halftone representation of the gray scale hologram can be used [98,99].

The holographic projection used as a lithographic technique with table top EUV lasers was recently demonstrated by Isoyan et al. [100]. In this experiment the CGH mask was coherently illuminated by the EUV laser and the reconstructed holographic image was

used to print a Si wafer coated with PMMA photoresist placed at the reconstruction distance (500 μm) from the CGH. The motif was a standard lithographic resolution test pattern with 1.54 μm lines and spaces. The field size of the mask is approximately 103 μm × 103 μm, and the pixel size 140 nm. An important step in the demonstration of this table top patterning technique was the mask design and fabrication. The mask was fabricated on an ultrathin membrane to achieve a reasonable high transmittance. The thickness of the membrane is a critical design parameter due to the high absorption that all materials have at the laser's wavelength. For this mask the supporting transparent membrane was a 25 nm thick SiNH, with a transmission $T \cong 13.5\%$ at 46.9 nm wavelength [93]. The membrane was coated with a 65 nm thick hydrogen silsesquioxane (HSQ) photoresist. The 65 nm thick layer of HSQ efficiently absorbs the radiation at 46.9 nm, with a transmission approximately 3% providing the necessary contrast to define the hologram. The CGH mask was defined in the photoresist by e-beam lithography.

6. Fabrication of nanostructures

The patterning techniques described in Sections 3–5 show the ability of the EUV lasers to be utilized as light sources to implement table-top photolithography tools capable of feature fabrication with nanometer resolution in the surface of photoresists. Defining the nanostructure in the photoresist by photolithography is the first step in the fabrication process of nanostructures. To complete the process, transferring the nanopattern onto the substrate can be obtained with different, well-established techniques. In the case of lift-off, a precise matching of the photoresist thickness to the height of the nanostructure is necessary and requires an exact control of the dose and an accurate knowledge of the penetration depth of the EUV photons in the photoresist. This is the fabrication approach pursued by Ottaviano et al. to define 200 nm spaced Ni strips on a Si wafer after the photolitographic step by IL with a Lloyd's mirror interferometer and a EUV 46.9 nm laser developed at University of L'Aquila [101].

Another approach to transfer the patterns from the photoresist mask into the substrate is ion beam etching. The photoresist mask is defined in the surface of the sample. Then it is exposed to a collimated ion beam that removes the non-protected regions of the sample. Using the Lloyd's mirror setup described in Section 3 for the photolithographic step a photoresist mask composed of regular lines was defined in a Au coated substrate and with anisotropic ion etching we fabricated regular lines in gold.

A fused silica substrate coated with 3 nm of chromium and 90 nm of gold was first coated with a flash (5 nm) layer of SiO_2 to improve the photoresist adhesion. Then a layer of 90 nm thick HSQ was deposited by spin coating and exposed with the IL setup described in Section 3. The sample was further processed in an ion beam etcher to transfer the lines printed in the photoresist down to the Au layer. Fig. 10 is an SEM micrograph of the lines fabricated with this method. The period is 190 nm (95 nm lines and spaces) and the area covered was approximately 300 μm wide a several millimeters long. The inset in the figure is an image of the structure obtained with a larger magnification. The grating is very well defined and demonstrates a complete nanofabrication process based on a table top EUV patterning tool.

It is also interesting to mention a non-conventional patterning approach that uses the high energy of the 46.9 nm photons of the EUV laser to modify the optical characteristics of LiF crystals to generate arrays of color centers by simple irradiation. This non-conventional

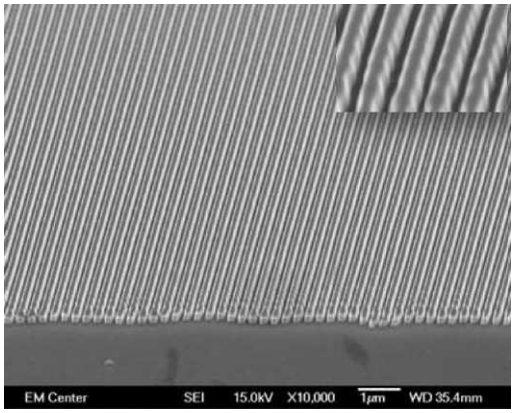

Fig. 10. SEM micrograph of 95 nm lines defined in a 90 nm thick Au layer. The structure was fabricated by ion beam etching using a photolithographic mask produced with the Lloyd's mirror interferometer. The inset is a detail of the structure obtained with larger magnification.

patterning technique has been used to demonstrate high resolution imaging and to create photo-luminescence gratings by EUV laser irradiation [54,102].

7. Summary

The recent development of compact EUV lasers enabled the realization of table top patterning tools with different configurations. Interferometric lithography is the patterning technique that better adapts to the highly coherent emission from the EUV table top laser sources. Based on the IL approach, both the amplitude division and wavefront division concepts were demonstrated in table top nanopatterning test-beds. The natural extension of the IL concept, the holographic projection lithography was also proved to be a viable way for arbitrary patterning with high resolution.

With the wavefront division scheme, lines and 2D structures were printed with exposure times of a few minutes over surfaces of the order of a fraction of one millimeter square. By changing the experimental conditions it was possible to modify the patterns from pillars to holes or print symmetric or elongated features with feature size down to 60 nm. Using an amplitude division scheme, lines with periods down to 95 nm were obtained. For this interferometer, however, the quality of the beam splitter is a limiting factor due to scattering that provokes a loss in the fringe contrast. The fabrication process of the beam splitters must be improved in order to reduce scattering centers and improve the modulation of the printed lines.

Holographic projection lithography was also demonstrated taking advantage of the highly coherent illumination of the EUV laser. This technique is very promising allowing arbitrary patterning with an extremely simple set up. The resolution in this case is limited by the size of the holographic mask that defines the NA of the exposure. Further development of high optical quality supporting membranes where the binary hologram is defined will allow to improve the resolution already demonstrated by this patterning technique.

The realization of a complete fabrication procedure for nanostructures using the table top EUV laser systems was also demonstrated. Gratings with 95 nm lines and spaces defined in a 90 nm thick layer of Au were defined by ion beam etching using a photoresist

mask printed by interferometric lithography with the table top EUV laser. Similar results in Cr were also demonstrated using the lift-off technique.

The present development of table top laser-pumped EUV lasers capable to emit in the region below 20 nm in combination with the photolithography tools described above can potentially further reduce the periods of the printed structures. The shorter wavelength lasers are obtained by irradiating a solid target with a short duration and high energy laser pulse to produce an elongated plasma column where strong gain is obtained in the $4d^1S_0$–$4p^1P_1$ transition of Ni-like ions in Ru, Pd, Ag, Cd, Sn, Sb and Te [103]. The possibility to utilize the shorter wavelength EUV laser sources in the applications described herein was recently favored by the enhancement of the beam spatial coherence achieved by seeding the plasma amplifiers with short wavelength high harmonic pulses [104,105]. The access to high brightness, short wavelength coherent laser sources will enable the demonstration of practical EUV IL tools for the quick fabrication of large arrays of periodic features in research oriented prototyping that so far was restricted to the use of large synchrotron facilities.

Acknowledgements

This work was supported by the NSF ERC for Extreme Ultraviolet Science and Technology, Award Number EEC-0310717 and NSF Award ECCS 0901806. The authors acknowledge the collaboration and fruitful discussions with colleagues and students who contributed in different ways to the results presented in this paper: A. Isoyan, F. Cerrina, L. Urbanski, M. Grisham, G. Vaschenko, M. Capeluto, S. Heinbush, D. Martz, W. Chao, E. Anderson, W. Rockward, D. Hill, J.J. Rocca, C.S. Menoni.

References

[1] W.J. Kaiser, L.D. Bell, Physical Review Letters 60 (1988) 1406–1409.
[2] G. Chen, Physical Review B 57 (1998) 14958–14973.
[3] A. Majumdar, Journal of Heat Transfer—Transactions of the ASME 115 (1993) 7–16.
[4] E. Betzig, J.K. Trautman, Science 257 (1992) 189–195.
[5] T. Ichimura, N. Hayazawa, M. Hashimoto, et al., Physical Review Letters 92 (2004).
[6] W. Srituravanich, N. Fang, C. Sun, et al., Nano Letters 4 (2004) 1085–1088.
[7] A.V. Zayats, A.A. Smolyaninov II, Physics Reports—Review Section of Physics Letters 408 (2005) 131–314.
[8] V. Pelletier, K. Asakawa, M.S. Wu, et al., Applied Physics Letters 88 (2006).
[9] E.E. Scime, E.H. Anderson, D.J. McComas, et al., Applied Optics 34 (1995) 648–654.
[10] G.A. Baker, D.S. Moore, Analytical and Bioanalytical Chemistry 382 (2005) 1751–1770.
[11] J.B. Jackson, N.J. Halas, Proceedings of the National Academy of Sciences of the United States of America 101 (2004) 17930–17935.
[12] R. Zia, J.A. Schuller, A. Chandran, et al., Materials Today 9 (2006) 20–27.
[13] J.J. Baumberg, T.A. Kelf, Y. Sugawara, et al., Nano Letters 5 (2005) 2262–2267.
[14] M. Campbell, D.N. Sharp, M.T. Harrison, et al., Nature 404 (2000) 53–56.
[15] W.J. Fan, S. Zhang, K.J. Malloy, et al., Journal of Vacuum Science & Technology B 23 (2005) 2700–2704.
[16] L.J. Heyderman, H.H. Solak, C. David, et al., Applied Physics Letters 85 (2004) 4989–4991.
[17] S.Y. Chou, P.R. Krauss, Journal of Applied Physics 79 (1996) 5066.
[18] F.B. Mancoff, N.D. Rizzo, B.N. Engel, et al., Nature 437 (2005) 393–395.
[19] C.N. Anderson, P.P. Naulleau, Journal of Vacuum Science & Technology B 27 (2009) 665–670.
[20] P.P. Naulleau, C.N. Anderson, J. Chiu, et al. 22-nm Half-pitch extreme ultraviolet node development at the SEMATECH Berkeley microfield exposure tool. 2009.
[21] J.A. Hoffnagle, W.D. Hinsberg, F.A. Houle, et al., Journal of Photopolymer Science and Technology 16 (2003) 373–379.

[22] J.A. Hoffnagle, W.D. Hinsberg, M. Sanchez, et al., Journal of Vacuum Science & Technology B 17 (1999) 3306–3309.
[23] E.H. Anderson, IEEE Journal of Quantum Electronics 42 (2006) 27–35.
[24] S.Y. Chou, P.R. Krauss, P.J. Renstrom, Journal Of Vacuum Science & Technology B 14 (1996) 4129–4133.
[25] S.Y. Chou, P.R. Krauss, P.J. Renstrom, Science 272 (1996) 85–87.
[26] C. Park, J. Yoon, E.L. ThomasPolymer 44 (2003) 7779.
[27] H. Schulz, D. Lyebyedyev, H.C. Scheer, et al., Journal of Vacuum Science & Technology B 18 (2000) 3582–3585.
[28] S.H. Zaidi, S.R.J. Brueck, Journal of Vacuum Science & Technology B 11 (1993) 658–666.
[29] H.H. Solak, C. David, Journal of Vacuum Science and Technology B 21 (2003) 2883–2887.
[30] H.H. Solak, C. David, J. Gobrecht, et al., Microelectronic Engineering 61–62 (2002) 77–82.
[31] H.H. Solak, C. David, J. Gobrecht, et al., Journal of Vacuum Science and Technology B 20 (2002) 2844–2848.
[32] A. Fernandez, J.Y. Decker, S.M. Herman, et al., Journal of Vacuum Science & Technology B 15 (1997) 2439–2443.
[33] A.K. Raub, D. Li, A. Frauenglass, et al. Fabrication of 22 nm half-pitch silicon lines by single-exposure self-aligned spatial-frequency doubling. 2007.
[34] J. Heck, D.T. Attwood, W. Meyer-Ilse, E.H. Anderson, Journal of X-Ray Science and Technology 8 (1998) 95–104.
[35] M. Switkes, M. Rothschild, Journal of Vacuum Science & Technology B 19 (2001) 2353–2356.
[36] M. Switkes, R.R. Kunz, M. Rothschild, et al., Journal of Vacuum Science and Technology B 21 (2003) 2794–2799.
[37] T.M. Bloomstein, M.F. Marchant, S. Deneault, et al., Optics Express 14 (2006) 6434–6443.
[38] A.K. Raub, A. Frauenglass, S.R.J. Brueck, et al., Journal of Vacuum Science & Technology B 22 (2004) 3459–3464.
[39] S.R.J. Brueck, Proceedings of the IEEE 93 (2005) 1704–1721.
[40] M. Fritze, T.M. Bloomstein, B. Tyrrell, et al., Solid State Technology 49 (2006) 41–43.
[41] R.R. Kunz, M. Switkes, R. Sinta, et al., Journal of Microlithography Microfabrication and Microsystems 3 (2004) 73–83.
[42] B.W. Smith, A. Bourov, H.Y. Kang, et al., Journal of Microlithography Microfabrication and Microsystems 3 (2004) 44–51.
[43] M. Switkes, M. Rothschild, Journal of Vacuum Science and Technology B 19 (2001) 2353–2356.
[44] M. Rothschild, T.M. Bloomstein, R.R. Kunz, et al., Journal of Vacuum Science & Technology B 22 (2004) 2877–2881.
[45] B.W. Smith, Y.F. Fan, J.M. Zhou, et al. Hyper NA water immersion lithography at 193 nm and 248 nm. 2004.
[46] J.J. Rocca, V. Shlyaptsev, F.G. Tomasel, et al., Physical Review Letters 73 (1994) 2192–2195.
[47] J.J. Rocca, F.G. Tomasel, M.C. Marconi, et al., Physics of Plasmas 2 (1995) 2547–2554.
[48] G. Tomassetti, A. Ritucci, A. Reale, et al., European Physical Journal D 19 (2002) 73–77.
[49] J. Filevich, M.C. Marconi, K. Kanizay, et al., Journal De Physique Iv 11 (2001) 483–486.
[50] F. Brizuela, G. Vaschenko, C. Brewer, et al., Optics Express 13 (2005) 3983–3988.
[51] M.G. Capeluto, G. Vaschenko, M. Grisham, et al., IEEE Transactions on Nanotechnology 5 (2006) 3–7.
[52] C.A. Brewer, F. Brizuela, P. Wachulak, et al., Optics Letters 33 (2008) 518–520.
[53] L. Juha, M. Bittner, D. Chvostova, et al., Applied Physics Letters 86 (2005).
[54] G. Tomassetti, A. Ritucci, A. Reale, et al., Applied Physics Letters 85 (2004) 4163–4165.
[55] S. Heinbuch, F. Dong, J.J. Rocca, et al., Journal of Chemical Physics 125 (2006).
[56] S. Heinbuch, F. Dong, J.J. Rocca, et al., Journal of Chemical Physics 126 (2007).
[57] M. Berrill, F. Brizuela, B. Langdon, et al. Warm photoionized plasmas created by soft-x-ray laser irradiation of solid targets. 2008.
[58] F. Brizuela, Y. Wang, C.A. Brewer, et al., Optics Letters 34 (2009) 271–273.
[59] G. Vaschenko, C. Brewer, E. Brizuela, et al., Optics Letters 31 (2006) 1214–1216.
[60] H. Bravo, B.T. Szapiro, P. Wachulak, et al., Nanometer scale machining by laser ablation with a focused extreme ultraviolet laser beam, in: Proceedings of the CLEO-IQEC 09. 2009: Baltimore.
[61] H. Bravo, B.T. Szapiro, P. Wachulak, et al., Nanometer scale machining with soft X-ray lasers, in: Proceedings of the soft X-ray lasers and applications. 2009: San Diego.
[62] S. Heinbuch, M. Grisham, D. Martz, et al., Optics Express 13 (2005) 4050–4055.
[63] B.R. Benware, C.D. Macchietto, C.H. Moreno, et al., Physical Review Letters 81 (1998) 5804–5807.
[64] M.C. Marconi, J.L.A. Chilla, C.H. Moreno, et al., Physical Review Letters 79 (1997) 2799–2802.

[65] Y. Liu, M. Seminario, F.G. Tomasel, et al., Physical Review A 6303 (2001).
[66] Y.W. Liu, M. Seminario, F.G. Tomasel, et al., Journal De Physique Iv 11 (2001) 123–126.
[67] J.W. Goodman, in: Statistical Optics, Wiley, New York, 1985.
[68] G. Tomassetti, A. Ritucci, A. Reale, et al., Optics Communications 231 (2004) 403–411.
[69] V.I. Ostashev, A.M. Gafarov, V.Y. Politov, et al., IEEE Transactions on Plasma Science 34 (2006) 2368–2376.
[70] N. Sakamoto, M. Masnavi, M. Nakajima, et al., Japanese Journal of Applied Physics 47 (2008) 2250–2258.
[71] Y.P. Zhao, Q. Wang, Y. Xie, et al., Journal of Plasma Physics 74 (2008) 839–846.
[72] C.A. Tan, K.H. Kwek, Journal of Physics D—Applied Physics 40 (2007) 4787–4792.
[73] A. Fernandez, D.W. Phillion, Applied Optics 37 (1998) 473–478.
[74] H.H. Solak, Microelectronic Engineering 78–79 (2005) 410–416.
[75] H.H. Solak, C. David, Journal of Vacuum Science & Technology B. 21 (2003) 2883–2887.
[76] A. Isoyan, A. Wuest, J. Wallace, et al., Optics Express 16 (2008) 9106–9111.
[77] H.H. Solak, D. He, W. Li, et al., Applied Physics Letters 75 (1999) 2328–2330.
[78] Y. Ekinci, H.H. Solak, C. Padeste, et al. 20 nm Line/space patterns in HSQ fabricated by EUV interference lithography. 2007.
[79] H.H. Solak, Y. Ekinci, P. Kaser, et al., Journal of Vacuum Science & Technology B 25 (2007) 91–95.
[80] A. Ritucci, A. Reale, P. Zuppella, et al., Journal of Applied Physics 102 (2007).
[81] P.W. Wachulak, M.G. Capeluto, M.C. Marconi, et al., Optics Express 15 (2007) 3465–3469.
[82] P.W. Wachulak, M.G. Capeluto, M.C. Marconi, et al., Journal of Vacuum Science & Technology B 25 (2007) 2094–2097.
[83] H.H. Solak, C. David, J. Gobrecht, et al., Microelectronic Engineering 67–68 (2003) 56–62.
[84] P.W. Wachulak, M.G. Capeluto, C.S. Menoni, et al., Opto-Electronics Review 16 (2008) 444–450.
[85] P. Wachulak, M. Grisham, D. Martz, S. Heinbuch, W. Rockward, D. Hill, J. Rocca, C.S. Menoni, E. Anderson, M.C. Marconi, Journal of the Optical Society of America B 25 (2008) B104–B107.
[87] A. Yen, E.H. Anderson, R.A. Ghanbari, et al., Applied Optics 31 (1992) 4540–4545.
[88] T.A. Savas, S.N. Shah, M.L. Schattenburg, et al., Journal of Vacuum Science & Technology B 13 (1995) 2732–2735.
[89] M. Switkes, T.M. Bloomstein, M. Rothschild, Applied Physics Letters 77 (2000) 3149–3151.
[90] T.A. Savas, M.L. Schattenburg, J.M. Carter, et al., Journal of Vacuum Science & Technology B 14 (1996) 4167–4170.
[92] D.P. Mancini, K.A. Gehoski, E. Ainley, et al., Journal of Vacuum Science & Technology B 20 (2002) 2896–2901.
[93] CXRO, http://www-cxro.lbl.gov/.
[94] C. Jacobsen, M. Howells, Journal of Vacuum Science & Technology B 10 (1992) 3177–3181.
[95] C. Jacobsen, M.R. Howells, Journal of Applied Physics 71 (1992) 2993–3001.
[96] A. Isoyan, Y.C. Cheng, F. Jiang, et al., Journal of Vacuum Science & Technology B 25 (2007) 2145–2150.
[97] M.R. Howells, C. Jacobsen, Applied Optics 30 (1991) 1580–1582.
[98] M.S. Fu, O.C. Au, Signal Processing—Image Communication 16 (2001) 909–930.
[99] G.Z. Yang, B.Z. Dong, B.Y. Gu, et al., Applied Optics 33 (1994) 209–218.
[100] A. Isoyan, F. Jiang, Y.C. Cheng, P. Wachulak, L. Urbanski, J.J. Rocca, C.S. Menoni, M.C. Marconi, F. Cerrina, SPIE Proceedings 7271 (2009) 72713O.
[101] L. Ottaviano, F. Bussolotti, S. Piperno, et al., Plasma Sources Science & Technology 17 (2008) Article Number: 024019.
[102] G. Tomassetti, A. Ritucci, A. Reale, et al., Europhysics Letters 63 (2003) 681–686.
[103] Y. Wang, M.A. Larotonda, B.M. Luther, et al., Physical Review A 72 (2005).
[104] Y. Wang, E. Granados, F. Pedaci, et al., Nature Photonics 2 (2008) 94–98.
[105] Y. Wang, E. Granados, M.A. Larotonda, et al., Physical Review Letters 97 (2006).